Made in United States of America
Reprinted from JOURNAL OF PHYSICAL OCEANOGRAPHY
Vol. 27, No. 1, January 1997

Geosat Data Assimilation with Application to the Eastern North Atlantic

DETLEF STAMMER*

Institut für Meereskunde, Düsternbrooker, Kiel, Germany

(Manuscript received 27 September 1994, in final form 16 April 1996)

ABSTRACT

An attempt is made to determine the three-dimensional ocean circulation from satellite altimeter measurements by assimilating Geosat sea surface height data into an eddy-resolving quasigeostrophic (QG) model of the eastern North Atlantic Ocean. Results are tested against independent information from hydrographic field observations and moored current meter data collected during the Geosat ERM. The comparison supports the concept of inferring aspects of the three-dimensional flow field from sea surface height observations by combining altimetric measurements with the dynamics of ocean circulation models.

A Holland-type QG model with open boundaries is set up on a 2000 km × 2000 km domain of the eastern North Atlantic between 25° and 45°N, 32° and 8°W. By using a simple nudging technique, about two years of Geosat altimeter data are assimilated into the model every five days as space–time objective analyses on the model grid. The error information resulting from the analysis is used during the assimilation procedure to account for data uncertainties. Results show an intense eddy field, which in the surface layer interacts with a meandering Azores Front. Compared to Geosat, the model leads to smoothed fields that follow the observations.

Model simulations are significantly correlated with hydrographic data from March 1988 and June 1989, both close to the surface and in the subsurface. Good agreement is also found between the model velocity fields and moored current meter data in the top two model layers. The agreement is visually weak in the bottom layer, although a coherence analysis reveals an agreement between the model simulation and current meter data over the full water column at periods exceeding 80 days.

1. Introduction

During the last decade satellite altimetry has become a powerful tool for observing and understanding the ocean circulation by providing global and continuous sea surface height (SSH) observations. It was shown that the altimeter signals even from Seasat and Geosat were capable of adequately representing ocean surface dynamics (e.g., Willebrand et al. 1990) and could be used to monitor the surface current fields (Gordon and Haxby 1990; Stammer et al. 1991).

However, it is not obvious how to reconstruct the flow field of the full water column, given only surface flow observations. The related problem of the observability of the 3D flow field from surface observations has lead to a controversial discussion and stimulated many investigations. Observations show that the vertical structure of the ocean is predominantly low mode (e.g., Müller and Siedler 1992; Fukumori and Wunsch 1991), which suggests that the interior ocean current field is effectively coupled to the sea surface. This is supported by results from numerical studies, which show that the abyssal flow field is constrained by the sea surface pressure boundary condition (e.g., Holland and Malanotte-Rizzoli 1989, hereafter HMR; Haines 1991). The combination of altimetric observations with numerical models should therefore allow one to construct the flow field over the full water column consistent with surface observations.

To assimilate altimeter data into numerical circulation models, various assimilation techniques with a wide range of complexity are available. Ghil and Malanotte-Rizzoli (1991) provide a comprehensive review of assimilation methods presently under use in the atmospheric and oceanographic context, and Anderson and Willebrand (1989) review their oceanographic applications. Inverse methods allow us to account for errors in both data and models and are all constrained and unconstrained model–data combinations. But for realistic problems on large space or time scales, optimization methods known to be useful, such as the Kalman filter smoother or the adjoint methods, overwhelm present-day computer resources. A few example applications in the context of altimetric data can be found in Moore (1991), Schröter et al. (1993), and Fukumori et

* Current affiliation: Department of Earth, Atmospheric, and Planetary Sciences, Massachusetts Institute of Technology, Cambridge, Massachusetts.

Corresponding author address: Dr. Detlef Stammer, Center for Meteorology and Physical Oceanography, Department of Earth, Atmospheric and Planetary Sciences, Massachusetts Institute of Technology 54-1518, Cambridge, MA 02139-4307.

al. (1993). Instead, simple methods like nudging or direct insertion have been used widely in feasibility studies, which aimed at reconstructing the interior ocean flow from surface data. Most of those studies are based on twin-experiments with quasigeostrophic (QG) models in which synthetic observations are assimilated (Hurlburt 1986; DeMey and Robinson 1987; Berry and Marshall 1989; Verron and Holland 1989; Holland and Malanotte-Rizzoli 1989; Haines 1991). But extended nudging techniques have also been developed recently, to assimilate altimeter data into primitive equation (PE) models (e.g., Mellor and Ezer 1991; Haines et al. 1993). Similar procedures were applied to realistic observations both with QG and PE models (e.g., Holland et al. 1992; White et al. 1990; Robinson et al. 1989; Oschlies and Willebrand 1995).

However, twin-experiments can be vastly unrealistic because synthetic observations are not contaminated by measurement errors and are perfectly consistent with the underlying model physics, both in its mean and eddy components. In addition, synthetic observations are available to arbitrarily high resolution in both space and time. These situations are much in contrast to realistic conditions. Altimeter data are provided only along subsatellite tracks and are not fully compatible with the underlying model. In addition, they are plagued by measurement errors and data loss. Thus, they provide only a crude estimate of the true space–time variability of the ocean, which, in general, will differ from that of the model. Moreover, the model mean field will differ from the observed mean state.

Under such circumstances, the ocean model has to play a much more crucial role in extracting the dynamical signal from the noisy data and in carrying the information into data-sparse areas, both horizontally (between subsatellite tracks and in data dropout areas) and vertically from the surface toward the interior ocean. Faced with these difficulties, it might be questioned if the earlier encouraging results from identical twin-experiments are applicable to the real world. Unfortunately, it was hardly possible to compare model results with in situ data, due to the lack of simultaneous subsurface observations.

This latter issue is addressed in this study, in which Geosat observations are assimilated into a regional eddy-resolving quasigeostrophic ocean circulation model of the Iberian Basin using a simple nudging technique (Verron and Holland 1989). Geosat anomalies are referenced to the mean dynamic surface topography provided by Robinson et al. (1979, henceforth RBS). The model's success in simulating the true ocean circulation in subsurface layers is tested subsequently against in situ hydrographic and current meter data.

In a parallel and much similar effort, Capotondi et al. (1995a,b) investigated the dynamical consequences of assimilating both time mean and time-varying components of sea surface height data in the Gulf Stream extension area. Mechanisms of the model adjustment and the characteristics of the resulting new mean state are investigated when both components are assimilated separately. It was shown that the model behavior in the presence of the surface constraint can be described in terms of vertical Foffonof modes. A prescribed mean surface component determines a distortion of the geostrophic contours in subsurface layers, which constrain the deep mean flow field. The intensity of the mean flow is specified by the inflow conditions, as well as eddy forcing and dissipation.

Many of those dynamical considerations regarding the constraining of the mean flow field by surface data are applicable to our study and will not be repeated here. Instead, the primary focus of this paper is to test the success of reconstructing the time-varying flow field in the full water column. Because the boundary current area is dynamically distinct from the eastern North Atlantic and because of differences in various technical details, we consider our approach in the eastern North Atlantic to be distinct from that of studies in the western Atlantic. Conclusions drawn from both studies are much in agreement, however.

This paper is organized as follows. Section 2 addresses problems related to regional circulation models, the model initialization, and the assimilation procedure. In section 3 results of the assimilation experiments are presented, and section 4 deals with the test of the model simulations using the independent information of hydrographic and current meter data.

2. The model and assimilation procedure

a. Model of the eastern North Atlantic

Our experiments are based on Holland's (1978) QG model of a closed basin, which was formulated for N arbitrary layers by Chow and Holland (1986). This QG model has been widely used during various eddy-resolving experiments with both closed and open boundaries. Holland (1986) gives a summary of many of those studies.

For the present study, the QG model was set up in a 2000 km $\times$ 2000 km model domain that covers the eastern North Atlantic, north of the Canary Islands and east of the Azores between 25° and 45°N, 8° and 32°W. The resolution is 10 km in the horizontal and three layers in the vertical. A time step of 5400 s was used. In the bottom layer, 20% of the realistic bottom topography, truncated above 2000-m depth, was included. Model parameters used during our experiments are listed in Table 1, most of which are based on earlier studies by Holland and Malanotte-Rizzoli (1989).

Figure 1a shows the real topography in the model domain. While the continental shelf is a natural boundary at the eastern side, the bathymetry is dominated by the Mid-Atlantic Ridge (MAR) in the west. In between, the ocean floor can be considered approximately level at a mean depth of about 4500 m. Various field studies

TABLE 1. Model parameters.

$L_x \times L_y$ = 2000 km × 2000 km	Basin dimensions
δ_x = 10 km	Grid length
δt = 5400 s	Time step
H_1 = 500 m	
H_2 = 1000 m	Layer thicknesses
H_3 = 3000 m	
ϕ_c = 35°N	Reference latitude
λ = 20°W	Reference longitude
$f_0 = 8.365 \times 10^{-5}$	Coriolis parameter at reference latitude
$\beta = 1.875 \times 10^{-11}$	Rate of change of Coriolis parameter with latitude
$A_4 = 8 \times 10^{9}$ m^4 s^{-1}	Biharmonic friction coefficient
$\epsilon = 1 \times 10^{-7}$ s^{-1}	Bottom friction coefficient
$g'_{1/2} = 9.63 \times 10^{-3}$ m s^{-2}	Stratification parameters $g(\Delta\rho/\rho_0)$
$g'_{3/2} = 1.95 \times 10^{-3}$ m s^{-2}	At interfaces between layers

have shown (e.g., Käse et al. 1986, 1989) that the hydrography in this area is dominated by a mesoscale eddy field superimposed on the permanent frontal structure of the Azores Current (AC). Using the hydrographic data of Robinson et al. (1979) from a 1500-dbar reference, the mean AC is observed in Fig. 1b to flow eastward at approximately 5 cm s^{-1}, near 43°N. The Portugal Current is also indicated near 40°N by an enhanced current speed east of 20°W.

Using an N-layer model, the vertical structure of the $(N-1)^{th}$ baroclinic mode leads to the appropriate discretization of the vertical layers (Flierl 1978). Figure 2a shows a mean σ_n profile calculated from the RBS data over the model domain together with its corresponding profile of the Brunt–Väisälä frequency

$$N = \sqrt{g\rho_0^{-1}\frac{\partial\rho}{\partial z}}. \tag{1}$$

Related profiles of the first three eigenmodes (barotropic and first two baroclinic) are displayed in Fig. 2b, which follow as a solution of the eigenvalue problem

$$\frac{\partial}{\partial z}\left[\left(\frac{f_0}{N^2}\right)\frac{\partial F}{\partial z}\right] + \lambda^2 F = 0, \tag{2}$$

subject to the boundary condition $\partial F/\partial z = 0$ at z=0, −H, assuming a mean ocean depth of $H = -4500$ m. Related Rossby radii of deformation $r_i = \lambda_i^{-1/2}$, i = 0, 1, 2 of r_0 = 2330 km, r_1 = 25.7 km, and r_2 = 10.3 km, respectively, are in agreement with Emery et al. (1984). Based on the structure of the second baroclinic mode (zero crossings are at 350 m and 1580 m, respectively) the depths of the three layers have been chosen as 500 m, 1000 m, and 3000 m, respectively. Together with layer-averaged densities this results in radii of the first and second baroclinic model modes of 26 and 13 km, respectively.

The regional nature of the model and the need to simulate the Azores frontal structure requires some thoughts on boundary conditions. To simulate only a fraction of the real ocean requires lateral boundary conditions that represent the influence of the large-scale basin circulation on the local model domain. We have used boundary conditions as suggested by Charney et al. (1950), which prescribe the model streamfunction

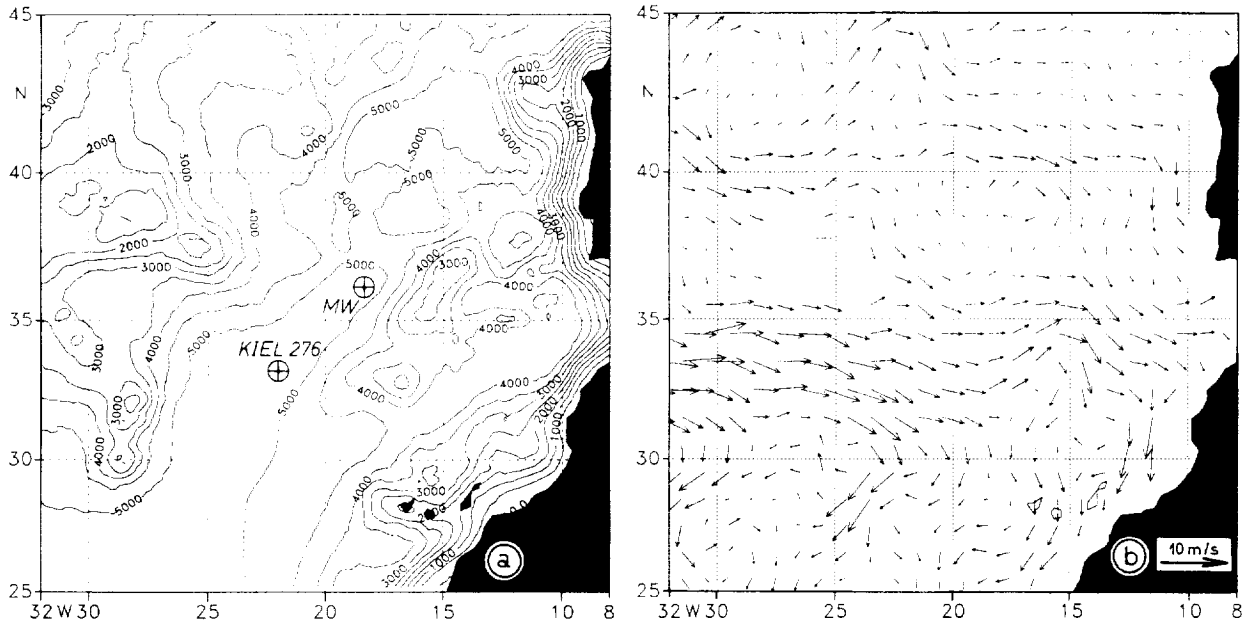

FIG. 1. (a) Realistic bottom topography in the model domain of the eastern North Atlantic. Marked are the positions of two moorings from which current meter data are used for model verification (compare Fig. 14). (b) Mean geostrophic surface circulation in 50 m relative to 1500 dbar as inferred from Robinson et al. (1979) climatologic atlas data.

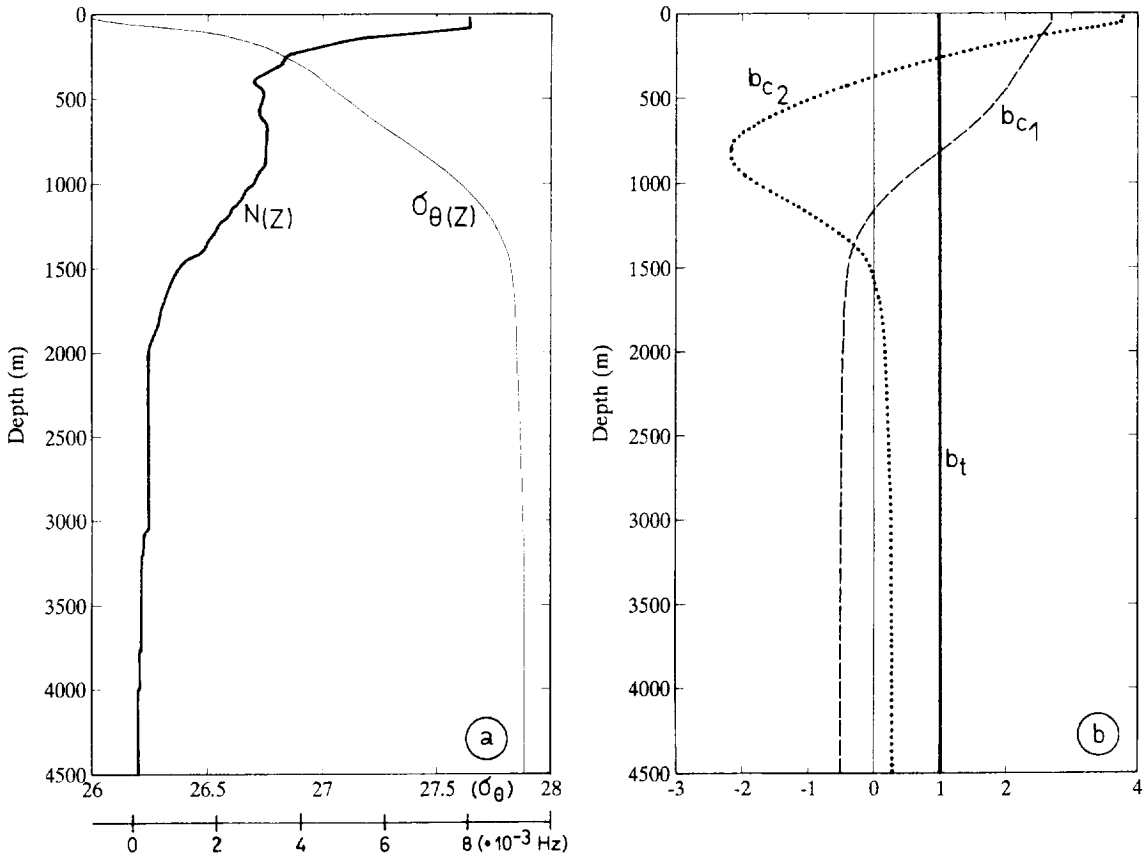

FIG. 2. (a) Mean profiles of potential density anomaly σ_θ and Brunt–Väisälä frequency N derived from the Robinson et al. (1979) hydrographic data for the model domain. (b) Barotropic and first two baroclinic vertical eigenfunctions.

Ψ_k and the relative vorticity $\zeta_k = \nabla^2\Psi_k$ on the complete boundary in each layer k during inflow. During outflow conditions, ζ is extrapolated from the interior model domain. Boundary conditions for Ψ and ζ are taken from the climatologic dynamic topography at the mean layer depths of the first and second layers (250 and 1000 dbar) determined from objective analyses of RBS atlas data relative to 1500 dbar (Fig. 4a, b). [Details on the analysis of the climatology are provided by Stammer et al. (1991).] Due to the lack of detailed information about the bottom layer, it is assumed to be at rest initially with no water entering or leaving subsequently.

In addition to lateral boundary conditions it is necessary to specify suitable surface boundary conditions, which also include the model forcing by the altimeter data. Generally, it is desirable to use a complete surface wind stress field taken simultaneously with the altimeter measurements. For example, daily ECMWF-model analyses would be a suitable source of wind data. But because of problems that arise in basically all models when simulating the Azores Front by real wind stress fields, we make the alternative assumption that the assimilation of altimeter data provides a vorticity source or sink at the surface equivalent to wind forcing, which is necessary to keep the model closely tied to the Geosat observations.

b. *Model initialization*

The relatively short periods over which real altimeter data exist and the regional nature of the model require a model initialization procedure that extrapolates the initial surface information into the deep layers in a dynamically consistent way that also takes the climatological background field into account. Various such approaches exist (e.g., see DeMey and Robinson 1987). Here we follow Holland et al. (1992), who used an initialization method based on the conservation of the QG potential vorticity Π in the interior ocean. During this procedure, the initial climatological potential vorticity fields Π_k from layers $k > 1$ are inverted jointly with an initially observed field Ψ_{obs} in the surface layer to infer a dynamically consistent set of model streamfunctions Ψ_1, Ψ_2, Ψ_3 and of potential vorticity Π_1, Π_2, Π_3 in the entire water column. This initialization assures that the potential vorticity of water particles, received initially from the climatological background, is consistent with subsequent source of Π during inflow con-

ditions. Haines (1991) uses a similar method to assimilate altimeter data into an ocean model through successive reinitialization.

Figures 3a and 3b display the climatological streamfunctions Ψ_p of the mean ocean circulation for layers 1 and 2, respectively, which have been inferred from RBS data based on the dynamic topography in 250 and 1000 dbar relative to 1500 dbar. The fields are dominated by the large-scale current structures within the model domain, with an inflow at the western boundary in both layers related to the eastward flowing Azores Current and to the extensions of the North Atlantic Current (NAC) in the northern part of the model domain. The resulting climatological potential vorticity fields Π_p for layers 1 through 3 are shown in Figs. 3c–3e, which are based on the assumption of a resting deep ocean. While the top layer is characterized by an enhanced horizontal Π gradient associated with the AC (Fig. 3c), the lower layers are dominated by the planetary potential vorticity (Fig. 3e).

Figures 4a, 4b, and 4f display the initial model streamfunction fields $\Psi(t_0)$ in the three model layers, which result from the inversion of the observations Ψ_{obs} (Fig. 4a) in the top layer and the subsurface climatological potential vorticity Π_p (Figs. 3d and 3e). The resulting initial eddy field relative to the climatological background (Fig. 4d to 4f) shows a strong vertical coherence with amplitude decreasing with depth by one order of magnitude and eddy scales increasing toward the bottom. During this type of model initialization, the surface eddy amplitude is projected predominantly onto the barotropic and first baroclinic mode, while the second baroclinic mode stays approximately unchanged.

c. *The assimilation procedure*

To assimilate altimeter data into the QG model, a simple Newtonian relaxation method ("nudging") is used. This technique has been used in many previous altimeter data assimilation studies and is extensively reviewed by Verron and Holland (1989) and Holland and Malanotte-Rizzoli (1989). In order to nudge the model streamfunction toward altimeter observations, the vorticity equation of the surface layer is extended to include the relaxation term $R(\nabla^2\Psi_{obs} - \nabla^2\Psi_1)$, where the QG streamfunction Ψ_{obs} is related to the altimeter observations h_{obs} of the surface elevation as

$$\Psi_{obs} = \frac{g}{f_0} h_{obs}. \tag{3}$$

The weight of the relaxation term relative to the model physics is determined by the timescale $\tau_r = R^{-1}$ and by the difference between the model and observations.

Empirically determined coefficients from twin-experiments suggest that τ_r should be of the order of ½ to 1 day (see HMR). The latter value has been used in the assimilation experiments of Holland et al. (1992) during which a QG model was nudged toward Geosat observations in the Agulhas retroflection area. Capotondi et al. (1995a,b) used τ_r = ½ day in the Gulf Stream region. A scale analysis shows that those numbers are about an order of magnitude smaller than all time scales of the remaining physical terms in the equation (see Capotondi et al. 1995a), which implies that the model surface streamfunction is effectively replaced by the observations.

However, real altimeter data are subject to a variety of errors that arise from such problems as incorrect environmental corrections or the lack of an instantaneous ocean background field. To account for those errors it seems plausible to use a somewhat reduced weight on the data by diminishing the relaxation coefficient to allow model physics to correct tendencies in the sea surface elevation that are not dynamically consistent. This issue will be addressed further below.

During all experiments, the observations h_{obs} were provided as a space–time objective analysis on the model grid every 5 days, estimated previously from the alongtrack data using correlation scales in space and time of λ = 100 km and τ = 15 days, respectively [see Stammer et al. (1991) for details on the objective analysis of the Geosat data]. The absolute surface elevation $h_{obs} = \bar{h} + h'$ was obtained from the sum of the Geosat anomalies h' and the climatologic dynamic topography $\bar{h}$ from the center of the first model layer at 250-m depth relative to 1500 dbar. An example of the resulting fields is shown in Fig. 4a.

To assimilate those altimetric fields, the relaxation coefficient R was modified to include a positive weighting function ϵ, and a Gaussian exponential in time to be $R = \epsilon R_0 \exp[(-\Delta t/\tau p)^2]$, where $\Delta t = t - t_{obs}$ is the distance between the model and the observations in time and τ_p is an exponential decay (persistence), which can be represented by the decorrelation time of the observations. From Geosat observations we estimated τ_p to be of the order of 5 days. The coefficient ϵ accounts for the Geosat estimation error provided by the objective analysis. It is close to unity where the uncertainty of the objective analysis is negligible, and it approaches zero when the analysis uncertainty is close to the process variance.

Instead of using objective analyses, one could also directly assimilate the alongtrack Geosat data. This approach has been successfully used by Verron (1992). Here we do not follow this method because it would constrain the model more by uncertainties than is the case when using the analyzed fields. This holds in particular for the tidal alias error (Schlax and Chelton 1994) by which an error signal is introduced with apparent westward phase propagation similar to first mode baroclinic Rossby waves. The tidal alias error is much reduced in the space–time objective analyses used in this study.

A schematic of the model setup is drawn in Fig. 5. The hatched area next to the boundaries indicates a friction layer that is built in to damp reflected planetary

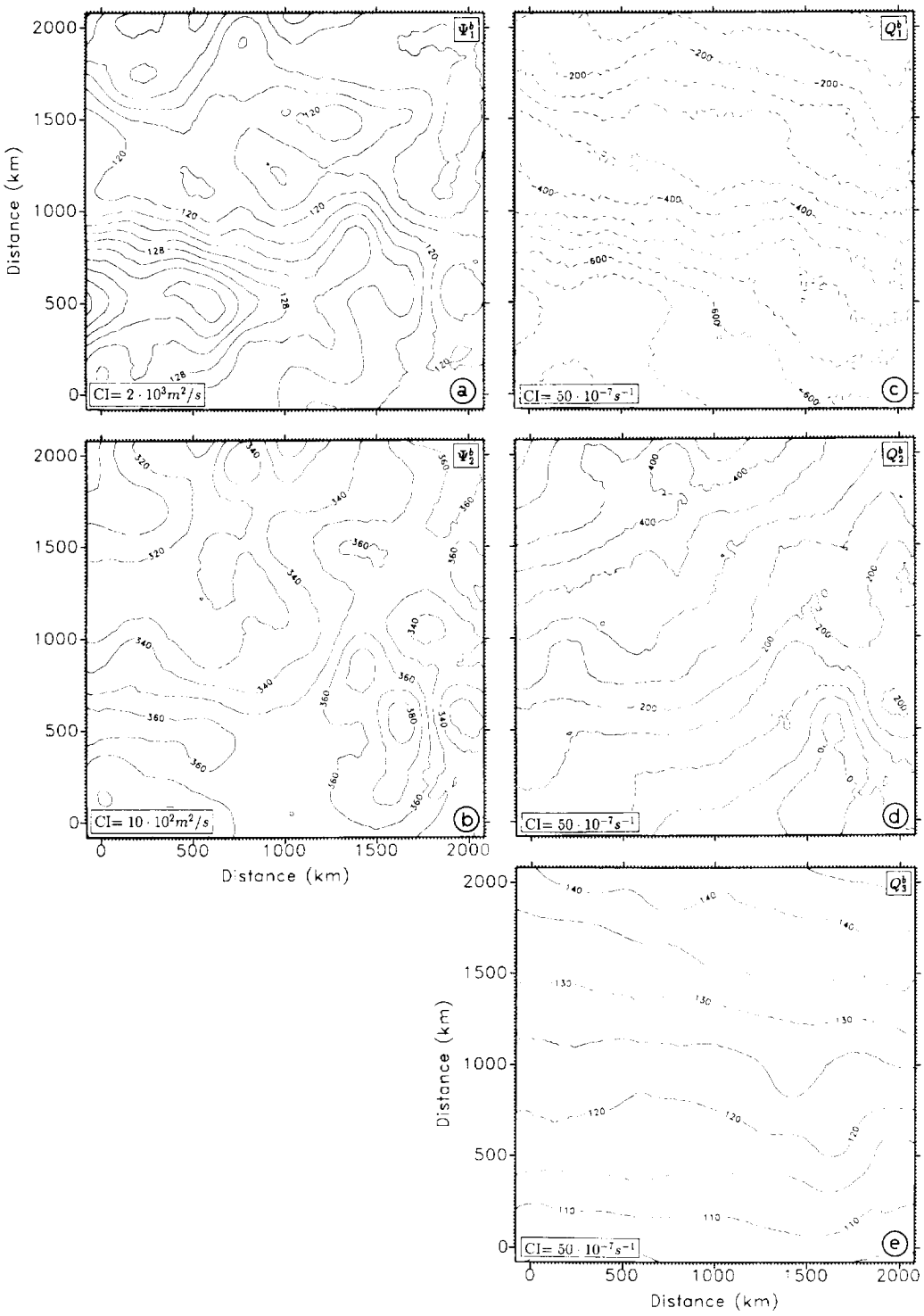

FIG. 3. (a) and (b) Mean fields of the climatological QG streamfunction Ψ_n in layer 1 and 2, which follow from the Robinson et al. (1979) dynamic topography in 250 and 1000 dbar, respectively, relative to 1500 dbar. The bottom layer is assumed to be resting. (c) to (e) Fields of climatologic potential vorticity Π_n based on the fields given in (a) and (b) and a resting bottom layer.

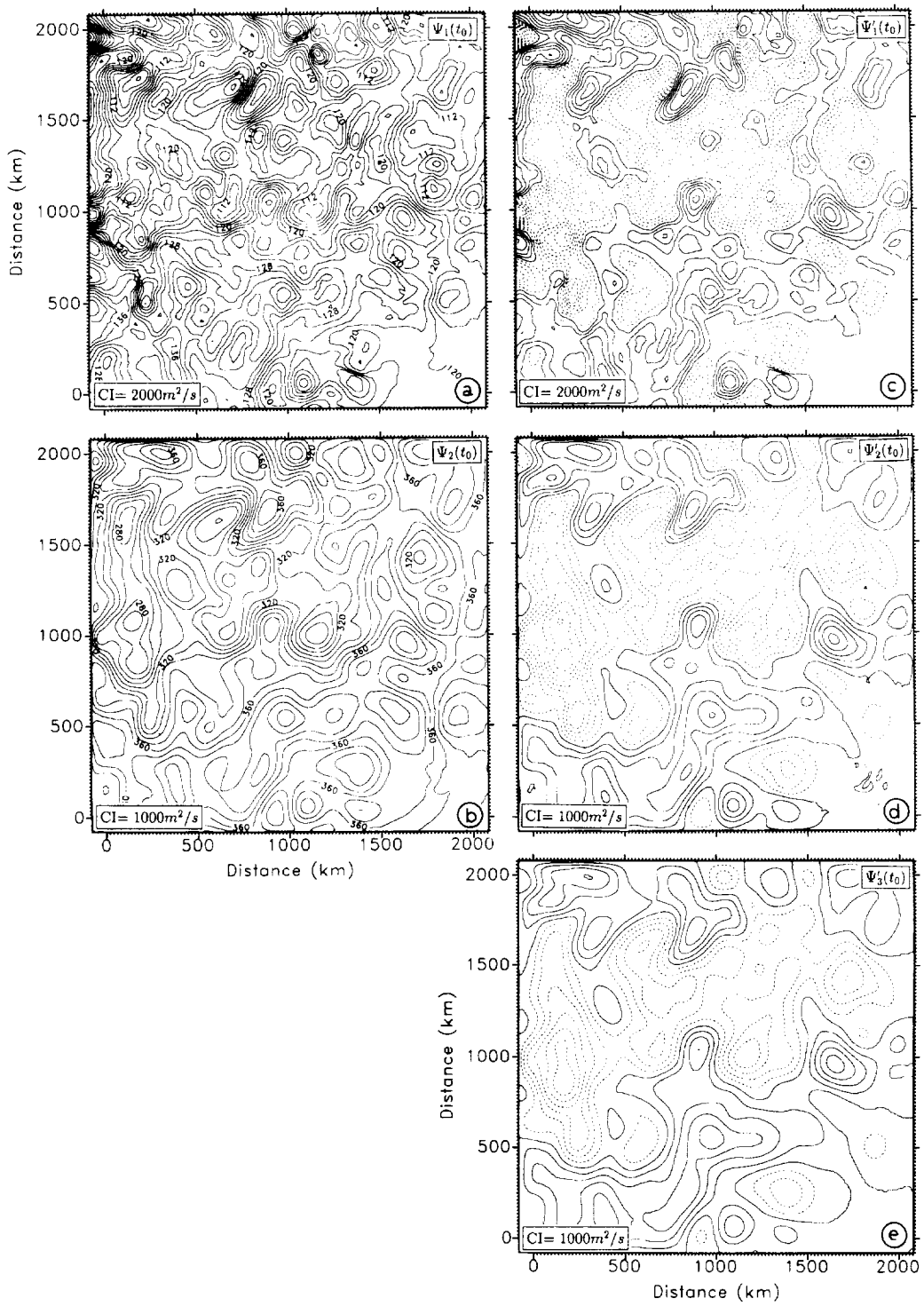

FIG. 4. Initial streamfunction $\Psi(t = t_0)$ on 15 August 1987 that results from Ψ_{obs} in the surface layer and the climatological potential vorticity in the two subsurface layers: (a) and (b) show the full streamfunction field in the top two layers. The initial eddy component in all three layers are given in (c)–(e), respectively.

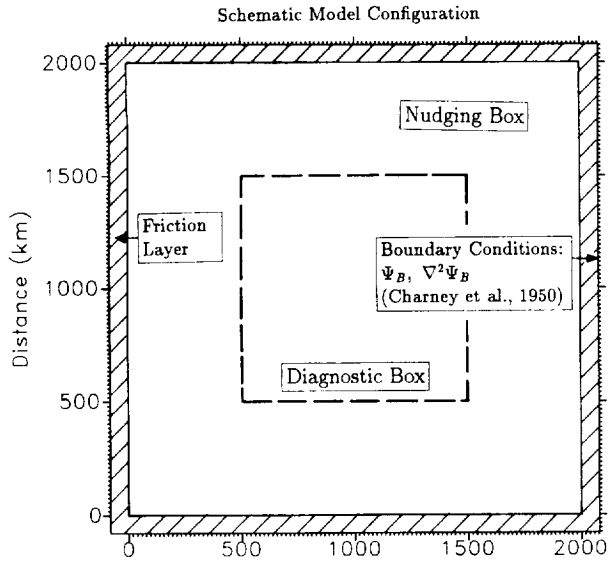

FIG. 5. Schematic of the regional QG model used in the assimilation study. The model streamfunction Ψ and vorticity $\nabla^2\Psi$ are specified on the boundaries from climatological hydrographic data; during outflow conditions the values for $\nabla^2\Psi$ are extrapolated onto the boundary from the interior model domain. Model mean quatities such as total kinetic energy were diagnosed in the interior dashed box with geographical limits of about 29.5°–40.5°N, 28°–12°W.

waves at the artificial boundaries. The damping is implemented by nudging the model fields toward the climatological background with a relaxation timescale linearly increasing from infinity to 100 days over the outer 10 grid points. The Geosat data are assimilated in the area enclosed by this 100-km wide friction layer. To avoid the influence of remaining boundary effects, integral properties like kinetic energy or model–data misfit were evaluated in the inner dashed box, with geographical extend from about 29.5° to 40.5°N, 28° to 12°W.

3. Model results

Starting from the initial model state given in Fig. 4, about two years of Geosat data were assimilated subsequently into the QG model. The initial and final times correspond to 15 August 1987 and 3 July 1989, respectively, giving a total period of 688 days.

In order to study the sensitivity of the results to the specific choice of the relaxation coefficient, R_0^{-1} was modified between 0.5 and 5 days. A summary of those experiments is given in Table 2. Figure 6a illustrates the model history during experiment N21 from the total kinetic energy, $T_k = \frac{1}{2}H_k\int\int(\nabla\Psi_k)^2\,dxdy$, in all three layers ($k$ = 1, 2, 3). Also included in the figure is the observed kinetic energy T_{obs}. Noticeable are the large, up to 30%, variations in the observed energy with periods of maximum and minimum energy coinciding with autumn and spring, respectively. The energy level in the surface layer decreases rapidly by about one-third during the first 50 days, but the model tracks the observed energy variations thereafter. The initial rapid decrease in T can be explained by the biharmonic friction that damps the energy on small scales present in both the Geosat analysis and the initial model field of the surface layer. Based on the biharmonic friction coefficient $a = 8 \times 10^9$ m^4 s^{-1}, the damping timescale for the near grid scale signals is of the order of 25 days (Holland 1978). In contrast to the top layer, where real observations are used as the initial field, no adjustment process can be found in the lower layers. Instead, the variations in T_2 and T_3 are relatively small throughout the assimilation period for

TABLE 2. Assimilation experiments and their parameters. Also shown are basin averages of model kinetic energy for all layers, as well as the mean rms model–data difference and cross correlation. Kinetic energy T in ergs per square centimeter.

Expt	τ_r (days)	τ_n (days)	$\overline{T}_{obs}$	$\overline{T}_1$	$\overline{T}_2$	$\overline{T}_3$	$\overline{\text{rms}\Delta\zeta}$ (cm)	$\bar{r}$
N½1	0.5	1	1.54	1.34	0.43	1.16	2.4	0.80
N11	1	1		1.16	0.33	0.82	2.6	0.74
N21	2	1		0.92	0.24	0.54	3.0	0.63
N51	5	1		0.57	0.15	0.28	3.5	0.47
N52	5	2		0.80	0.21	0.21	3.2	0.59
SD	∞	—		0.46	0.13	0.19	4.7	0.02

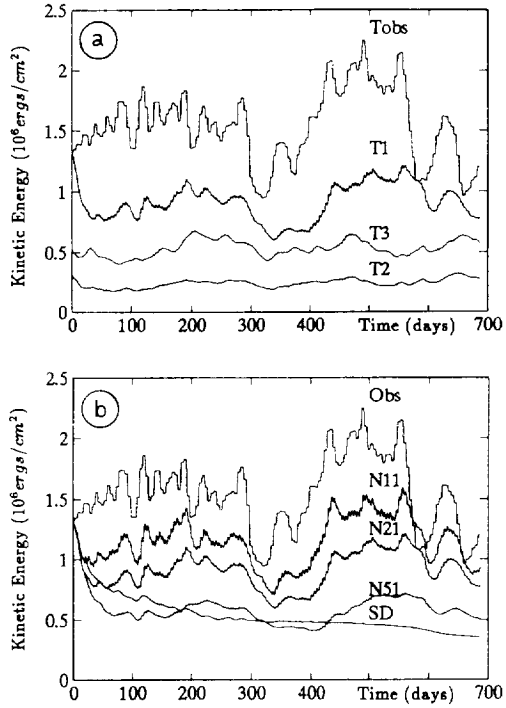

FIG. 6. (a) Total kinetic energy $T_k = \frac{1}{2}H_k\int\int(\nabla\Psi_k\,dx_k)\,dy$ in the three layers k obtained from experiment N21 as the spatial average within the inner dashed rectangle shown in Fig. 5. Also included in the figure is the observed kinetic energy T_{obs} from Geosat data. (b) Area-averaged kinetic energy T_1 of the surface layer that results from varying the relaxation coefficient between R^{-1} = 1 day and R^{-1} = 5 days. The curve labeled Obs shows the observed energy similar to (a), and SD stems from the unforced reference run. Labels refer to experiments and parameters listed in Table 2.

this choice of parameters. Fluctuations on the nudging timescale are subordinate, and a direct relation of variations in T_2 and T_3 with those observed cannot be found.

To illustrate the sensitivity of the model energy to the magnitude of the nudging parameter, Fig. 6b shows the surface layer kinetic energy T_1 from experiments with R_0^{-1} varying from 1 day to ∞. Note that the run, labeled "SD" (spin down), with $R_0^{-1} = \infty$ is driven only by the initial and lateral boundary conditions, with no data assimilated, and is provided here as an unforced reference.

As can be expected from Fig. 6b, the model energy decreases significantly with increasing relaxation time scale and for experiment N51 an energy level is approached, which is equivalent to the unforced run SD. During this experiment the forcing of the nudging term is roughly balanced by its dissipative effect on basin average. The frictional character of the nudging term is illustrated in the figure from the initial decrease in T_i which is significantly faster for all nudging experiments than for SD. Note the lag of the model behind observed variations in energy, which increases with decreasing coefficient R_0.

Figure 7 shows mean fields of Ψ (Figs. 7a–c) and Π (Figs. 7g–i) together with the variances of Π (Figs. 7d–f), as they result from experiment N21 in all model layers, respectively (from top to bottom). The mean model state is in general agreement with the climatology but leads to smoother fields. Note that the near-surface frontal structure associated with the AC has become sharper through the data assimilation, and that in contrast to the a priori assumption of a resting bottom layer, Fig. 7c shows a westward Azores Undercurrent of about 0.5 cm s^{-1}. The influence of the bottom topography on the abyssal mean circulation is especially clear in the western model domain where the Ψ contours basically follow the bathymetry of the MAR.

Maximum kinetic energy can be found along the AC in the top layer (Fig. 7d), with values continually decreasing in downstream direction. The enhanced variability in the upper left corner is related to an extension of the NAC, which is branching at that location into the Portugal Current. Contrary to the top layer, an increasingly homogeneous energy distribution in the meridional direction is found in the subsurface.

An analysis of the relative contribution of the various terms in the governing equations shows that the nudging term is dominating the model physics throughout the entire assimilation period with no apparent decreasing tendency. This implies an incompatibility between model and data. The related discrepancy in eddy characteristics between the model and observations is apparent from the left column of Fig. 8 showing instantaneous fields of the streamfunction from N21 of all three model layers at day 210 after a one-half-year period of data assimilation (12 March 1988). Similar fields from the unforced run SD are shown in the right column of the figure for reference. With data assimilation, the upper layer is dominated by strong eddy activity with maximum scales and amplitudes associated with the meandering AC frontal structure (Fig. 8a). A comparison with Fig. 4a indicates that eddy scales are significantly longer in the model than observed. Going from top to bottom, eddy amplitudes decrease and their scales increase. But, compared to the initial fields (Fig. 4), the eddy scales in the deep layers have been reduced through the continuous data assimilation, and the pronounced initial vertical coherence has vanished. Without any assimilation, model fields are uncorrelated with those from the assimilation run soon after the initialization. Dominant scales are increasing with time and ultimately reach values three times larger than those observed (see Fig. 9). In addition, the eddy amplitudes are decreasing significantly, especially in the eastern part of the model domain.

A phase diagram (Hovmöller diagram) of the eddy field, which is given in Fig. 9 from Ψ anomalies of both runs N21 and SD (relative to their 2-year mean) along 35°N, indicates a predominantly westward propagation of eddy structures. In good agreement with the underlying altimeter observations, phase velocities inferred from N21 are roughly 1.85 cm s^{-1} in the surface layer (Fig. 9a). However, values are increasing toward the bottom. In the second layer (Fig. 9b), values of 2 cm s^{-1} can be deduced. The westward propagating baroclinic structures are broken up by much faster perturbations, which make it difficult to estimate phase velocities in the bottom layer (Fig. 9c). Those vertically coherent and fast fluctuations, which do not show up with continuous nudging on the full model domain (not shown), are dominant during several periods of low data coverage (compare Fig. 11c). Note that similar but much more vigorous fluctuations are apparent in the unforced case SD during the initial adjustment period of the model after which the model has drifted into a completely different frequency–wavenumber regime than imposed by the observations.

For a comparison of the model results with Geosat observations, Fig. 10 shows the observed sea surface elevation h_{obs} (Fig. 10a) and its corresponding eddy signal h' (Fig. 10b), together with the resulting model fields from experiment N21 (Figs. 10c and 10d). Again, the model eddy fields are taken to be the anomaly relative to their 2-year mean and both fields correspond to 12 March 1988 (day 210). Areas of large data uncertainty (with an estimated error exceeding 60% of the process variance) are hatched in Fig. 10a. They are found predominantly in the eastern basin, where there is substantial data loss. High amplitude anomalies present in both observations and the model fields are much different in their spatial characteristics: while the observations are dominated by anomalies with large meridional extent, the model tends to form isolated eddies. This difference can be understood from the fact that vorticity ($\zeta = \nabla^2\Psi$) is assimilated rather than Ψ by which larger scales are suppressed in the model results.

The root-mean-square difference between both fields is about 2.5 cm and the cross-correlation is $r \approx 0.7$.

The rms difference and the cross-correlation between model and data eddy fields are given in Fig. 11 for the full assimilation period as a function of time. To indicate the range obtained from varying the relaxation timescale R_0^{-1}, results from experiments N11 and N51 are displayed. In the two cases, rms differences vary between 2 and 4 cm and are significantly lower than an upper threshold limit of 6 cm (labeled "Obs"), which indicates the differences of the observations relative to their initial field (persistence). Those latter values are reached asymtotically after the first 50 days of experiment SD, indicating the loss of correlation of the unconstrained run with the observations over that timescale.

In order to give a rough estimate of the data coverage during the assimilation, Fig. 11c shows the number of valid daily Geosat observations over the model area. It is clear that periods of increased model errors and reduced cross-correlation coincide with periods of significantly reduced data coverage. During those periods when up to 50% of the model grid is unforced by the altimetry, the fast transients, visible in Fig. 9, significantly degrade the agreements. A parameter $\tau_r = 1$ day is sufficient to keep the cross-correlation as high as $r = 0.8$, but the increased value of $\tau_r = 5$ days does not suffice to keep the model on track with the data during periods of massive data loss.

4. Model–data comparison

We proceed now with a test of the model simulations from experiment N21 against simultaneous and independent subsurface information available from hydrographic measurements and current meter data. Datasets used during the comparison are listed in Table 3.

a. Hydrographic data

Hydrographic data were measured on an eddy resolving grid during two cruises in March 1988 (Käse et al. 1989) and in May–June 1989 (Hinrichsen et al. 1993). The dynamic topography obtained from those data is used here as the observational counterpart of the model streamfunction. The data measured during March 1988 were obtained during a 3 week period between 4 and 26 March. Figures 12e,f show objective analyses of the resulting dynamic topography at 50 and 1000 dbar relative to 3000 dbar, respectively (see Käse et al. 1989 for details on the analysis). To allow a comparison with the model eddy field, the RBS climatology was subtracted from the hydrography.

Shown in Figs. 12a,b is the eddy field from the Geosat analysis and its error map, taken from 12 March 1988 (day 210). Figures 12c and 12d show the corresponding model eddy fields from layer 1 and layer 2, respectively. Discrepancies between the model simulations and the corresponding in situ measurements are, in particular, obvious close to the areas of enhanced observational errors. But otherwise the positions of various cyclonic and anticyclonic model eddies (labeled by capital and lowercase letters, respectively) and their scales are compatible with the hydrography in both layers. It has been shown that the anticyclones A to D are the surface signal of subsurface meddies (Käse et al 1989; Stammer et al. 1991). In contrast to the observations, however, feature B is separated from C by a trough and a second positive anomaly C′ is connected to A and C by a ridge. Similarly, positions and scales of the simulated cyclones a–d agree with the observations. Note that in contrast to the Geosat analysis (Fig. 12a) the model is able to simulate the observed positive anomaly B. In the second layer the amplitudes of the model eddies are significantly lower than have been observed, but their positions agree.

The correlation between the model fields and the hydrography of $r=0.58$ and $r=0.51$ in both layers, respectively, is found to be rather low, but still significant on the 95% confidence level. (Our comparison is based on the objective analysis of the field data on a 50 km $\times$ 50 km grid. In order to evaluate the confidence test, we used only those 120 grid points that are close to the actual station positions. Due to the correlation scale of $\lambda = 100$ km used during the hydrographic analysis, we considered only one-fourth of the grid points to be independent, which leads to an effective degree of freedom of 30.) Without data assimilation, no significant agreement of the model simulations with the observed hydrography is found ($r < .1$).

For a description of the ocean state during the time of the second cruise see Hinrichsen et al. (1993). During that period, Geosat has lost substantial amounts of data in the model domain (compare Fig. 13b), and a direct comparison of both datasets is not possible. Now the model dynamics have to carry all information into the data-sparse areas, which renders the comparison of the model results with the hydrography much more stringent. Results are shown in Fig. 13 with the model and altimeter fields taken from 21 May 1989. The hydrography resembles the dynamic topography 50 and 800 dbar relative to 2000 dbar. As in Fig. 12, only the eddy signal is shown. Although not directly forced close to the hydrographic station net, the model fields generally resemble a spatially coherent picture of structures, which to some degree represent the field data. As an example, the features B and B′ are simulated by the model in both layers, though with much reduced amplitudes. The corresponding correlations between model fields and the hydrography is $r=0.51$ and $r = 0.40$, for the first and second layer, respectively. This is slightly below that during the 1988 survey, but still significant.

b. Current meter data

Time series of moored current meter data are available from the central model domain (see Fig. 1a) and allow

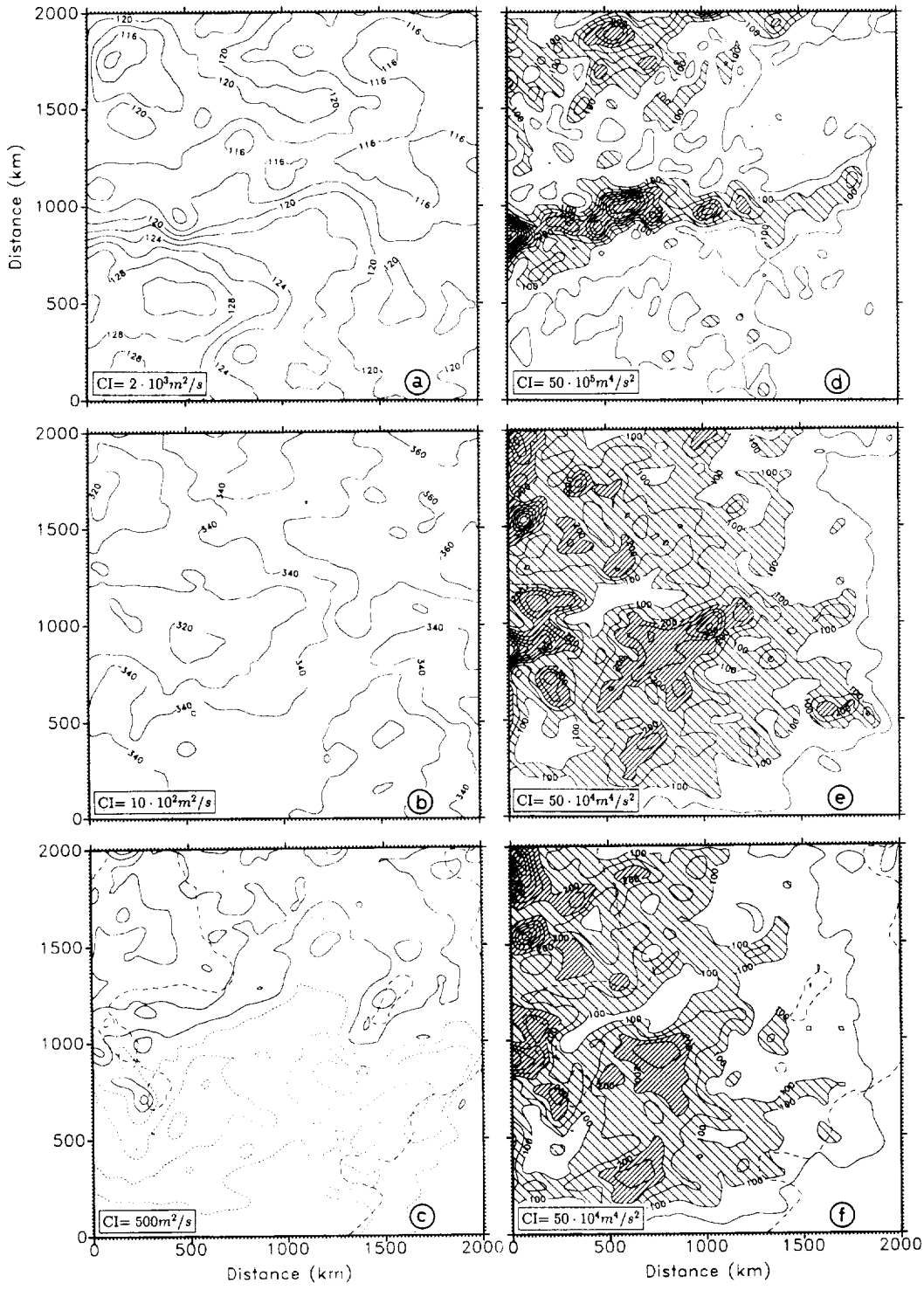

FIG. 7. (a)–(c) Mean model geostrophic streamfunction Ψ_k for layer k = 1, 2, 3, respectively, and (d)–(f) the related streamfunction variance evaluated over the 2-year long assimilation period of experiment N21. (g)–(i) The mean model potential vorticity fields for layer 1 through 3. The dashed line in (c) shows the 3000-dbar depth contour.

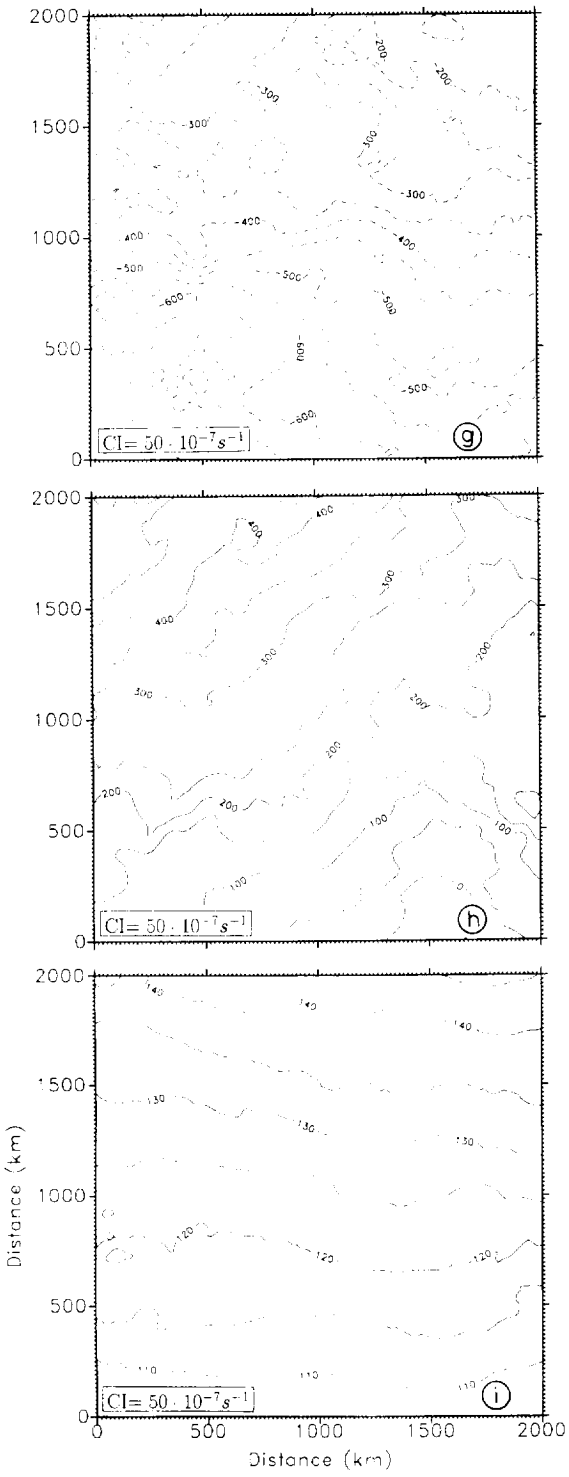

FIG. 7. (*Continued*)

a comparison with velocity fields from all three model layers. Zenk et al. (1989) and Müller and Siedler (1992) provide a detailed description of the current meter data. Previously, these data have been used in a direct comparison with Geosat geostrophic surface velocity estimates (Stammer et al. 1991; Stammer 1992). They will be used here to test the velocity in the subsurface model layers. Since the data from mooring "MW" were recovered only above 1000-m depth, the following comparison is based predominantly on data from mooring "Kiel276." But some results from mooring "MW" are included in Table 4.

Figure 14 shows the model velocities from experiment N21, subsampled once per day at the position of Kiel276 together with the observations. While the current meters at depth 1050 and 3000 m coincide with the mean depth of layer 2 and layer 3, the observations at 450-m depth stem from a depth range that is rather close to the interface between the top two layers. Statistics of all time series are listed in Table 4. The mean model velocities are of the same order as the observed values, but the model kinetic energy is lower by a factor of 2–3 than the observed—much in agreement with previous results (compare Fig. 6).

Despite the initial discrepancies between model and mooring velocities, which are likewise present between the mooring data and Geosat observations (Stammer 1992), a reasonably good agreement is found between both datasets in the top two model layers, with observed velocity fluctuations being simulated by the model even on small time scales. A good example can be found in Figs. 14a,b around 10 June 1988. However, the model–data agreement is weak in the bottom layer. A similar result was found by Capotondi et al. (1995b) from their assimilation experiment in the Gulf Stream extension area. It was shown there that the model-simulated eddy signal is significantly correlated with current meter data down to about 1500-m depth but the agreement became insignificant below.

Variance spectra of the velocity time series allow an analysis of frequency bands of enhanced agreement or disagreement. Shown in Fig. 15 are corresponding spectra of the v (northward) component. In layer 1 spectra from observed and simulated velocity time series agree on the 95% confidence level, and both follow roughly a -2 to -3 power law. Discrepancies between both are apparent only at frequencies above the nudging frequency (2×10^{-1} day^{-1}). On the contrary, the spectra from the deeper layers indicate systematic differences between the model and observations on all frequencies.

In order to determine those parts of the spectra that are strongly affected by the surface constraints, results from the unforced experiment SD are included in the figure. (Similar to experiment N21, spectra from SD characterize only that data period covered by the mooring data; thus the initial adjustment processes are excluded.) It follows that in all layers the model kinetic energy is significantly modified by the surface boundary conditions. In the surface layer a surplus of model energy through assimilation reaches one to two orders of magnitude at all frequencies, while in layer 2 and layer 3 the increase is found to be limited to frequencies below

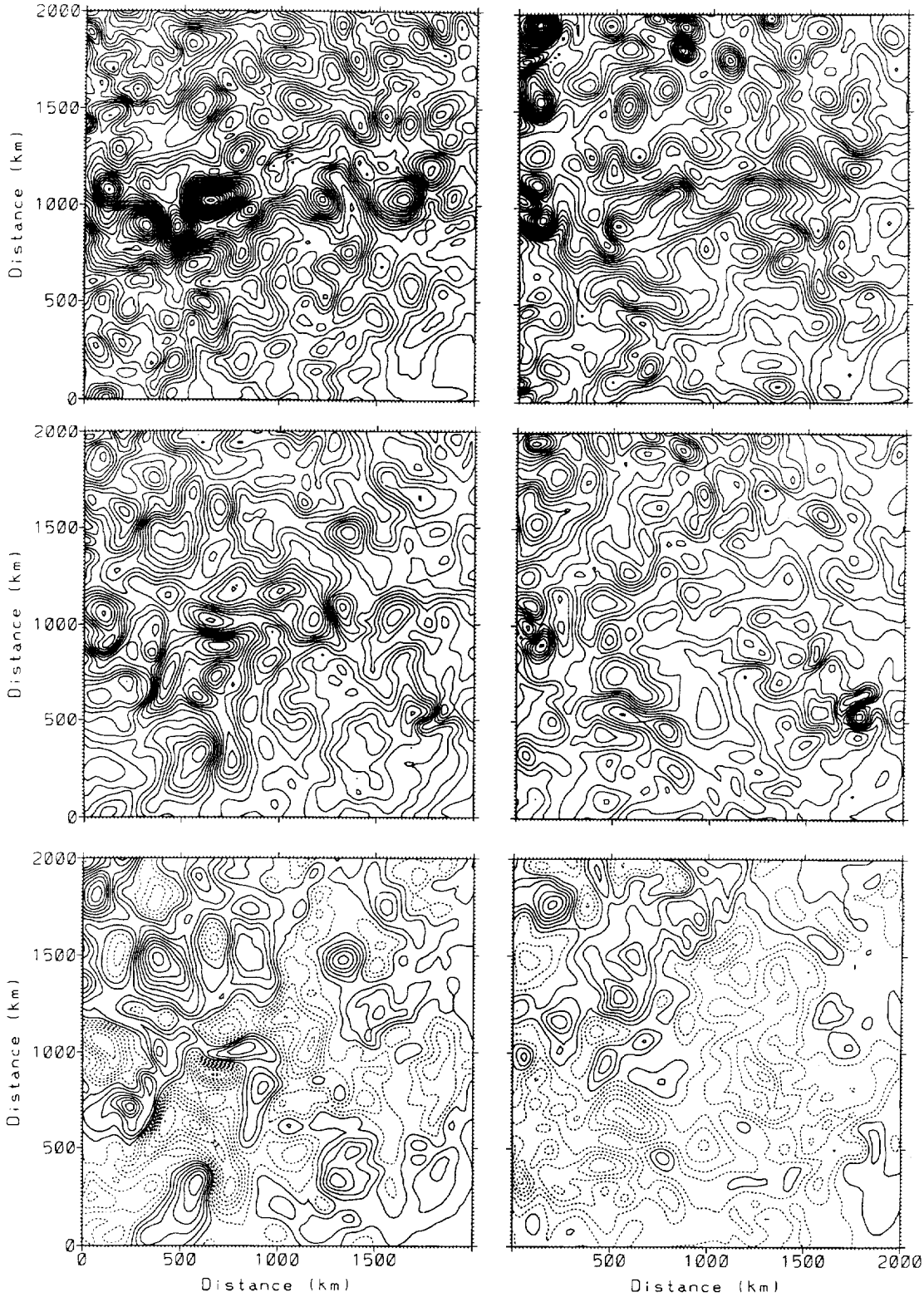

FIG. 8. (a)–(c) Instantaneous fields of the streamfunction taken after about 6 months of assimilation from experiment N21 at day 210 (12 March 1988) in the three model layers, respectively (top to bottom). Corresponding fields from experiment SD are shown in the right column. Contour intervals are 1000, 500, and 500 $m^2 s^{-1}$ from top to bottom in both columns.

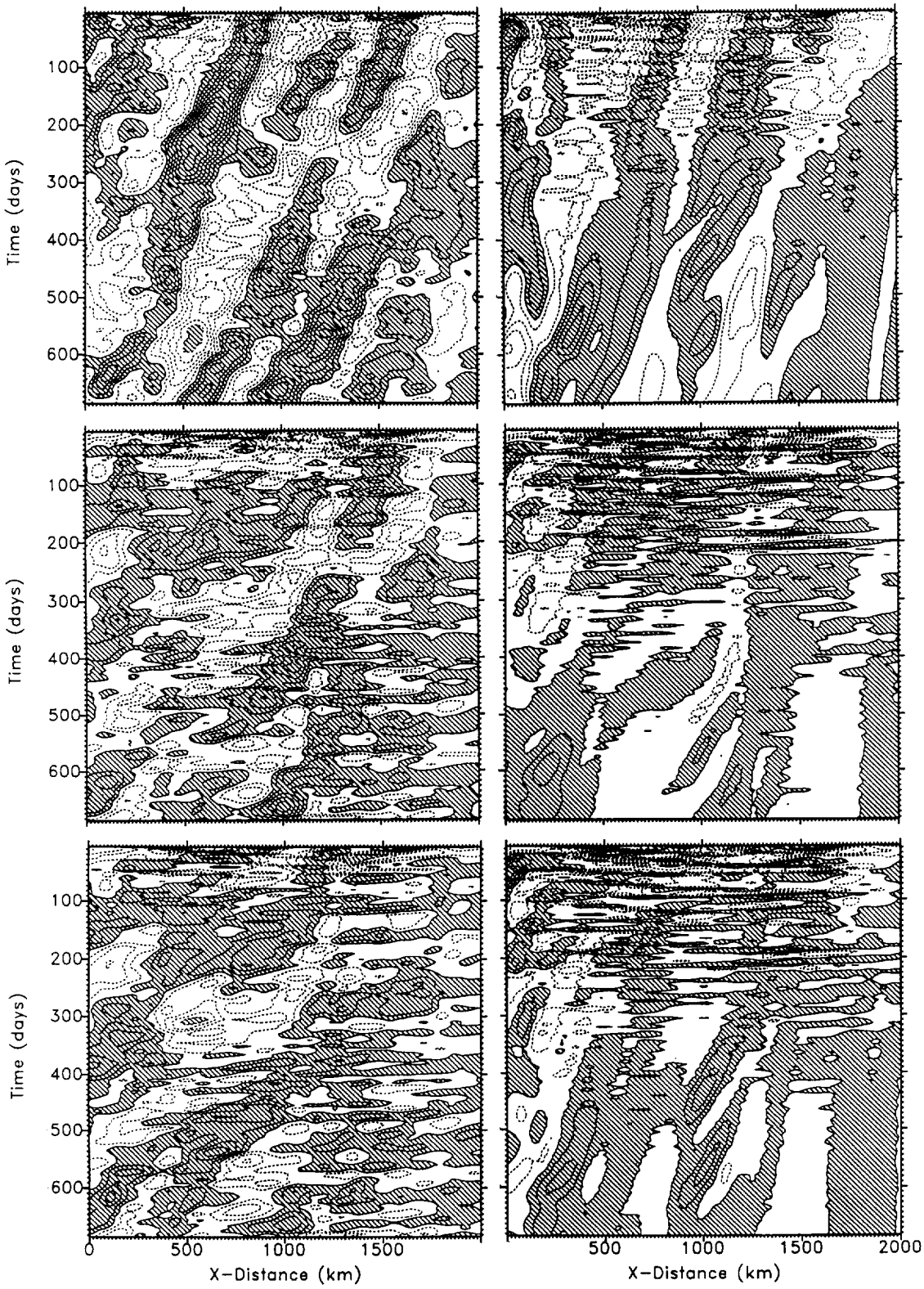

FIG. 9. Phase diagram showing the model eddy field referenced to the 2-year model mean given in Figs. 7a to 7c and plotted along $y = 1000$ km (about 35°N) as a function of time for all three model layers (top to bottom). Results are taken from experiment N21 in the left column (a to c) and positive areas are hatched. Panels (d)–(f) show corresponding fields from experiment SD.

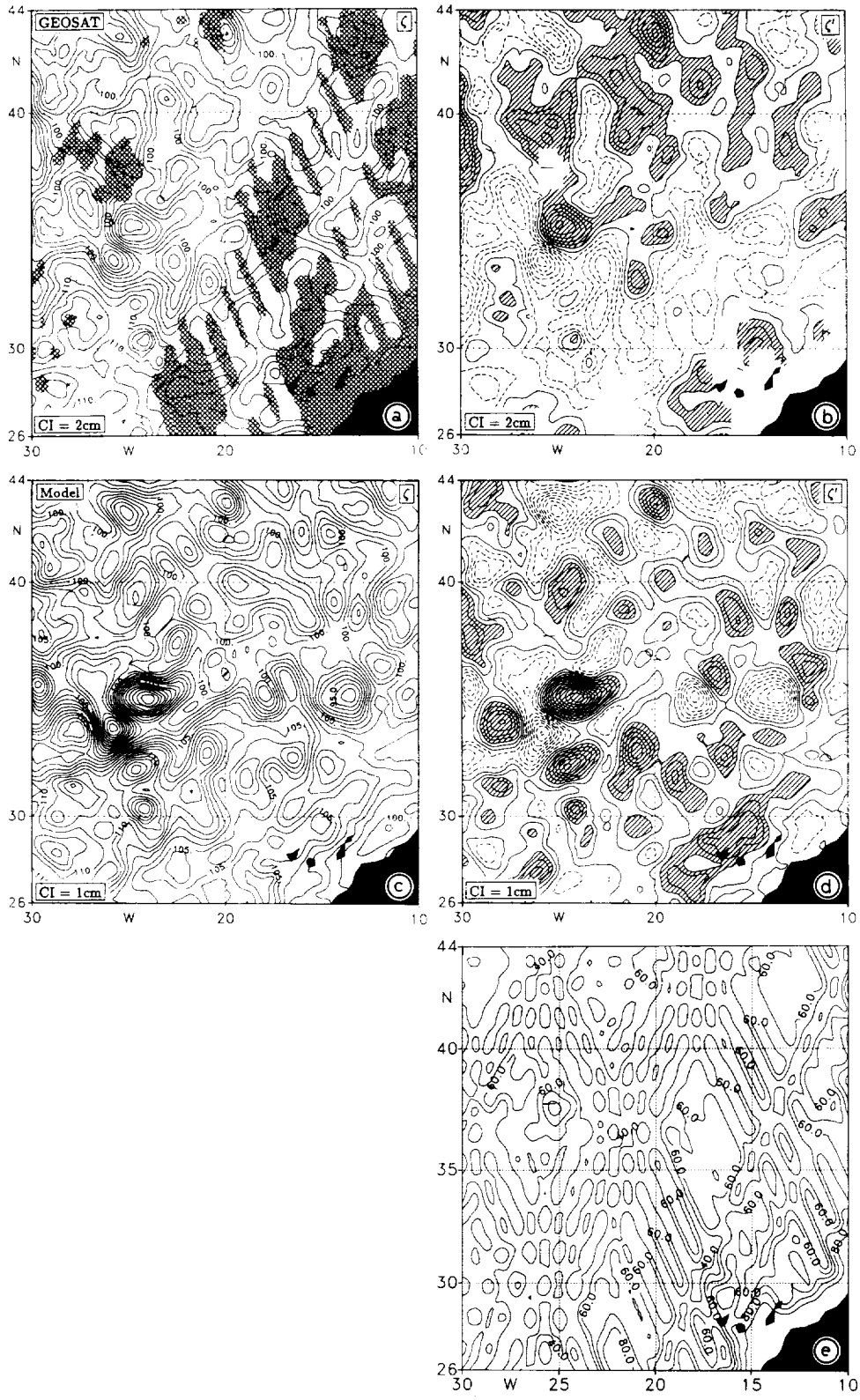

FIG. 10. (a) Absolute Geosat SSH field and (b) its eddy part at day 210 (12 March 1988). Instantanous fields of the absolute equivalent model elevation $\zeta = g^{-1} f_0 \Psi_1$ from experiment N21 at day 210 (12 March 1988) and its eddy part are shown in (c) and (d). Panel (e) shows the estimation error provided by the objective analysis for this specific instance and that is used during the assimilation procedure to weight the data quality. Hatched areas in Fig. 10a indicate regions where the error exceeds 60%.

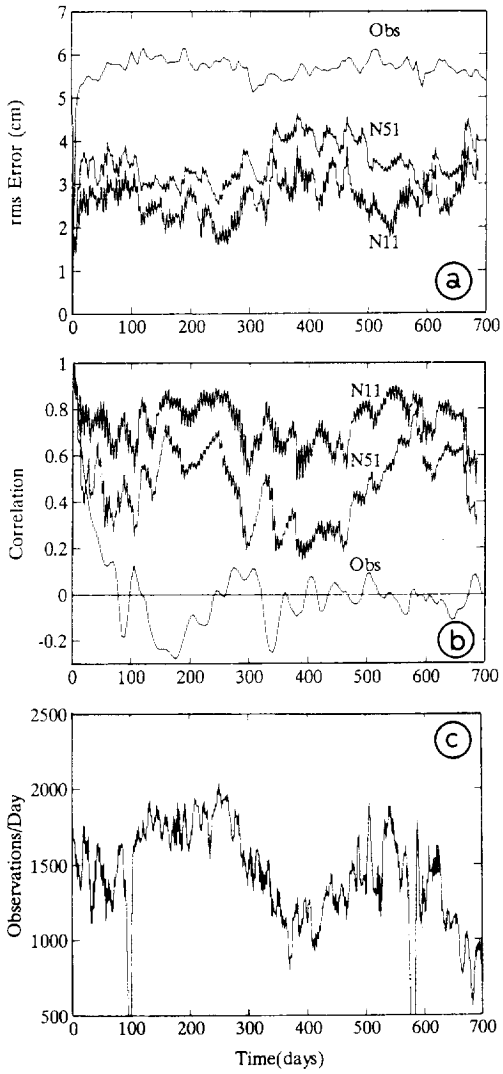

FIG. 11. (a) Rms model–data misfit as a function of time from experiments N11 and N51. Also included is the rms misfit of the observations with its initial field as a function of time (labeled Obs). In (b) the cross-correlations from the corresponding fields are given. The curve labeled Obs in (b) shows the data persistence, that is, correlation of the observations with the initial field as a function of time. (c) Number of valid Geosat 1-Hz measurements in the model domain as a function of time. Note the pronounced correlation between periods of increased misfit and reduced data coverage.

4×10^{-2} cpd. In addition, a pronounced energy peak can be found near the nudging frequency in all layers. It is possible that the limitation of the energy increase to periods exceeding about 25 days is related to the dynamical response of the model to the bandpassed surface observations. It is likewise possible that this finding is associated with the baroclinic response of the model to the surface observations (Frankignoul and Müller 1979).

Although a visual comparison does not indicate an agreement between the two velocity time series in the bottom layer, a coherence analysis reveals a significant coherence between model and mooring data in all layers at periods exceeding 80 days (Fig. 16). However, the analysis indicates also a peculiar phase lag, with the model leading the observations by 60° and 90° in layer 2 and layer 3, respectively. This finding is puzzling but may indicate a systematic discrepancy between model and data: due to the low vertical resolution the barotropic mode presumably is getting too much energy during the data incorporation, which results in unrealistically high phase speeds of induced eddy structures with relatively large scale. It is noteworthy that those phase lags are very sensitive to the presence of bottom topography. Without prescribed topographic structures, basically no coherence was found in the deep layers and topography with increasing amplitude leads to a decreasing phase lag of the deep model relative to observations.

TABLE 3. List of available in situ datasets.

	Comment
	Hydrographic data
4.3.–26.3.1988	67 hydrographic stations on an eddy-resolving grid mean station spacing < 60 km (Käse et al. 1989)
24.5.–20.6.1989	Hydrographic measurements on an eddy-resolving station grid (Hinrichsen et al. 1993)
	Mooring data
4.11.1987–8.1.1989	Mooring MW (36°8.4′N, 18°23.4′W): lowpass filtered daily mean current measurements in 630 and 1034-m depth
10.11.1987–10.1.1989	Mooring Kiel 276 (33°8.5′N, 21°57.6′W): lowpass filtered daily mean current measurements in 450/630-m, 1050/1250-m and 3000-m depth (Zenk et al. 1989)

5. Summary and concluding remarks

Perhaps the most important result from this study is that we find a significant correlation between simulated and observed structures of the ocean flow field in the eastern North Atlantic after constraining the model by Geosat surface SSH observations. This result is lending strong support to the hypothesis that even under realistic conditions at least aspects of the upper thermocline flow field of the ocean may be determined by combining sea surface observations with the physics of a numerical circulation model. Although studied extensively during various previous process studies using synthetic observations, it was never possible to test the earlier encouraging findings based on real data. The basic conclusion that can be drawn from this study is that the results from process studies are indeed consistent with those found under realistic conditions.

The assimilation of total surface elevation obtained from the sum of a climatological mean dynamic topog-

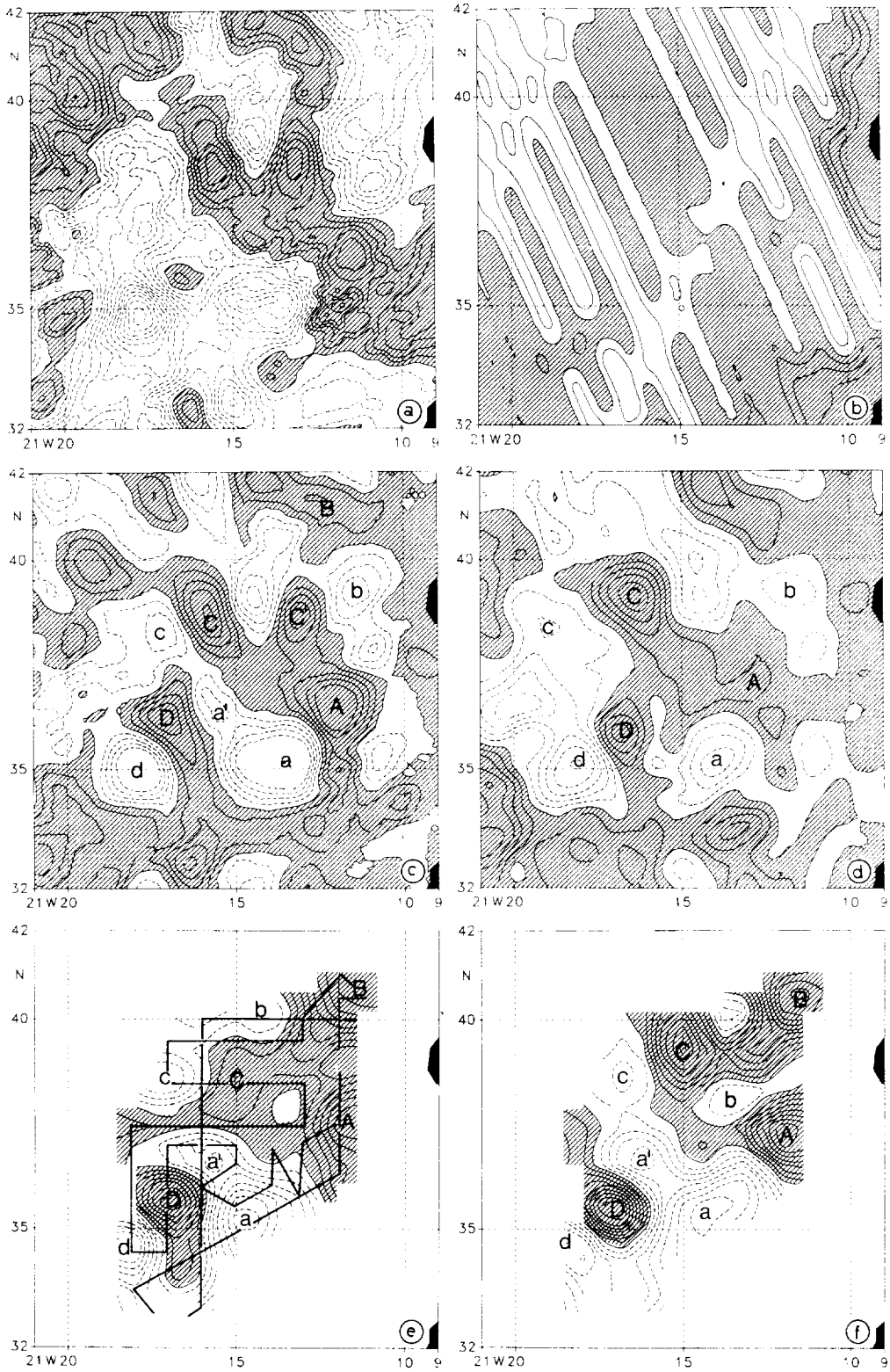

FIG. 12. (a) Geosat anomalies and model eddy field from the first (c) and second (d) layer, respectively, as they result for day 210 (12 March 1988). The hydrographic dynamic topography 50/3000 and 1000/3000 dbar is shown in panel (e) and (f), respectively, after the subtraction of the RBS climatologic dynamic topography fields. Positive values are hatched and cyclonic and anticyclonic eddy structures are labeled accordingly. In (b) the Geosat estimation error is given. Hatched areas indicate an estimation error exceeding 60% of the process variance. The cruise track is given in (e).

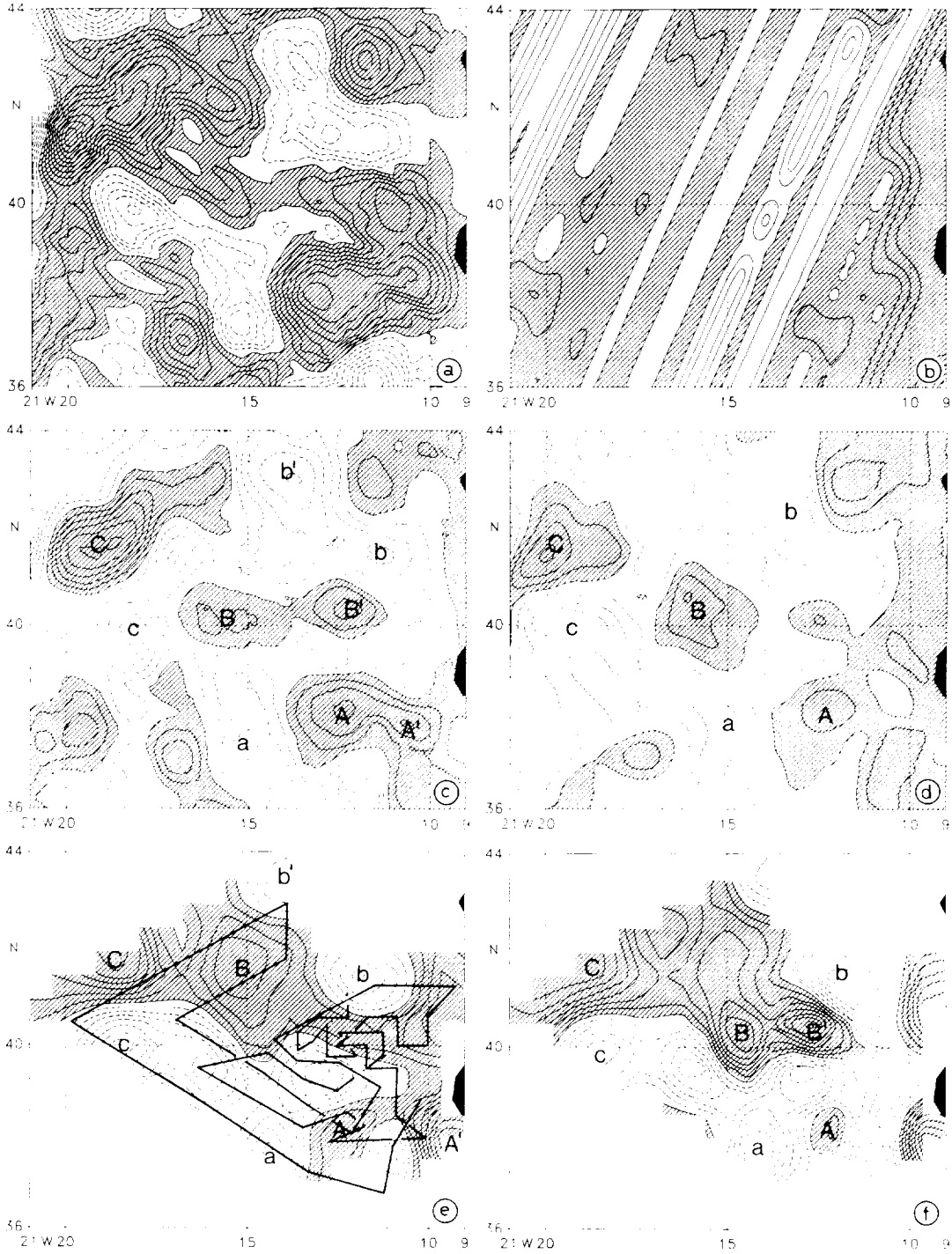

FIG. 13. As in Fig. 12 but for the hydrography obtained during the period 21 May to 20 June 1989. Shown is the dynamic topography (e) 20/2000 dbar and (f) 800/2000 dbar, respectively. Geosat and model results stem from 21 March 1989.

raphy and Geosat SSH anomalies leads to a mean model state consistent with the initial a priori climatology in all model layers. It is shown that the simulated current field is consistent with hydrographic observations of the ocean state in the top two model layers. A significant coherence is also obtained between model velocities and time series from moored current meter data over most of the water column on time scales exceeding 80 days. The comparison with an unforced reference run indicates that the model is constrained by the surface ob-

TABLE 4. Comparison of model results with mooring data. Listed are mean values and standard deviations of the zonal (u) and meridional (v) velocity components from the moorings and corresponding model simulations.

	Mooring				Model			
Layer	$\bar{u}$ (cm)	σ_u^2 (cm^2)	$\bar{v}$ (cm)	σ_v^2 (cm^2)	$\bar{u}$ (cm)	σ_u^2 (cm^2)	$\bar{v}$ (cm)	σ_v^2 (cm^2)
				1) Mooring MW				
S1	1.3	16	0.5	6	3.6	12	0.9	13
S2	0.6	7	0.4	3	0.6	2	0.2	1
				2) Mooring Kiel 276				
S1	0.4	11	−0.3	16	1.3	8	−1.3	22
S2	−0.2	3	−0.3	7	0.4	1	0.1	2
S3	−0.6	1	−0.2	1	−0.3	1	−0.1	1

servations in all layers, leading to enhanced energy on small time and space scales. No agreement can be found between simulations and in situ data without the data constraint in both the surface and subsurface layers.

In a parallel effort, Capotondi (1995a,b) assimilated Geosat altimetry into a QG model of the Gulf Stream extension area and compared resulting fields with various types of simultaneous in situ observations. Although their focus was on the improvement of the climatological behavior of the model as a consequence of the assimilated mean surface observations, their conclusions are in agreement with those presented here. In their study it was shown that the model-simulated eddy signal is significantly correlated with current meter data down to about 1500-m depth, but hardly below. It should be recalled, however, that due to the long adjustment time scale of the deep ocean potential vorticity, the convergence timescale toward the true state is much longer at depth than near the surface, even during twin exper-

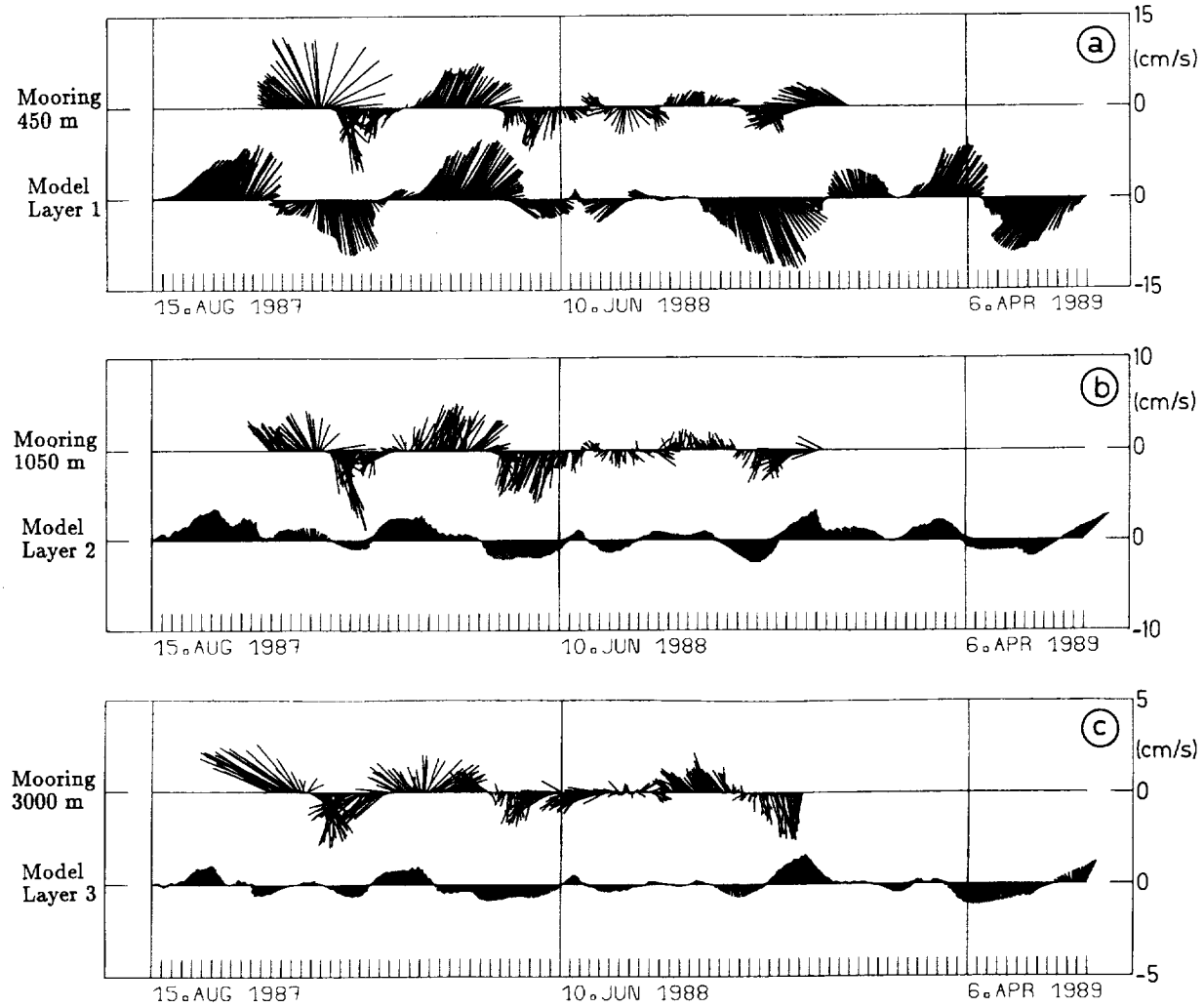

FIG. 14. Vector time series of daily model velocities subsampled from experiment N21 at the position of mooring Kiel276. Also included are the corresponding vector time series from the mooring at 450 m, 1050 m, and 3000 m, respectively.

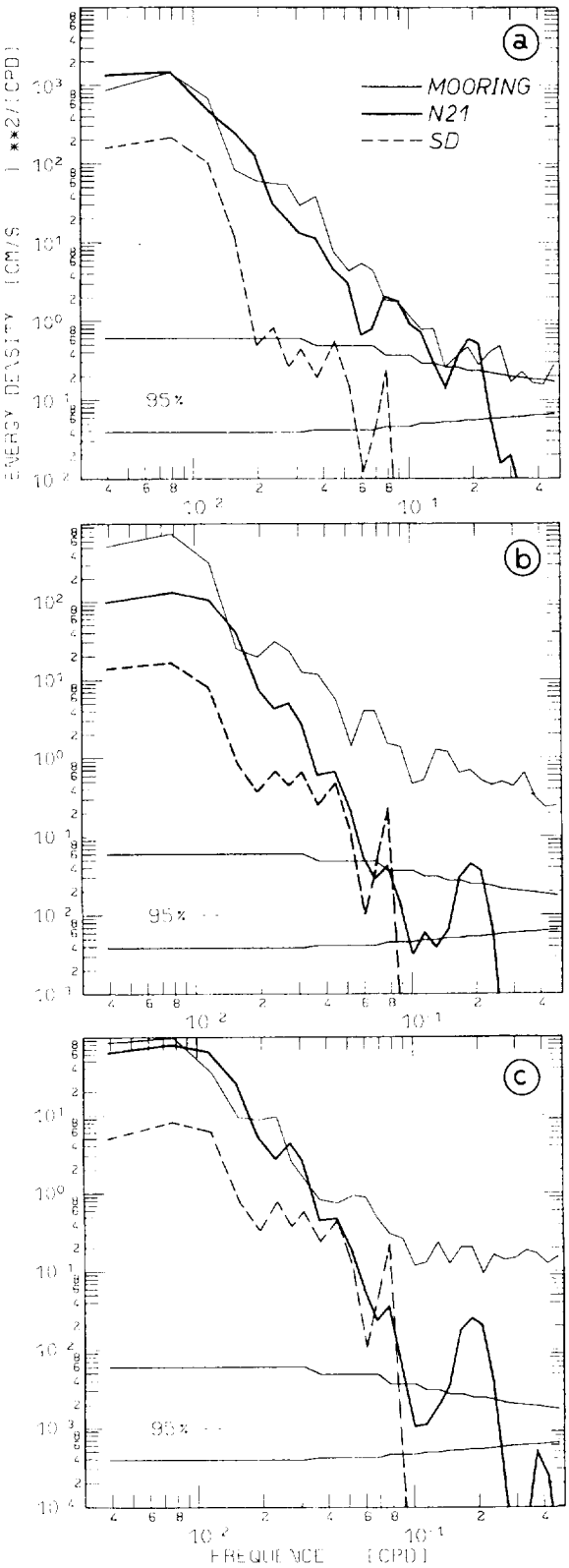

FIG. 15. (a) to (c) Variance density spectra of the v (northward) velocity component given in Fig. 14 from the mooring data (thin solid line) and experiment N21 (bold solid) in all three layers, respectively (from top to bottom). Also included are similar curves resulting from the reference experiment SD (dashed line).

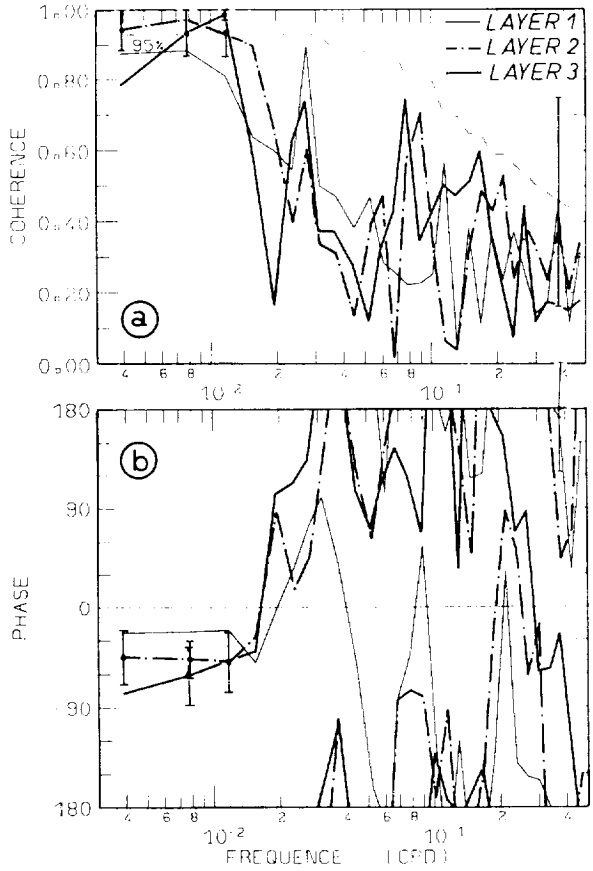

FIG. 16. (a) Coherence analysis between the v (northward) velocity component of the current meter data and model simulations given in Fig. 14. (b) Same as (a) but for the phase with observations leading for positive phase. In both panels thin solid, dash-dotted, and bold solid lines show results from layer 1, 2, and 3, respectively.

iments (e.g., see HMR). Therefore, the poor agreement of the simulations here, and in Capotondi et al. (1995b), could partly be due to the relatively short duration of the experiments.

Limits of present attempts in simulating the observed state of the ocean can be attributed to the poor quality of the Geosat altimeter data (observational errors and data distribution) and the limited representation of ocean dynamics in the regional QG model. Both shortcomings will be vastly improved in the near future. See, for example, Oschlies and Willebrand (1995) for a related attempt to assimilate Geosat data into the eddy-resolving Community Modeling Effort model of the North Atlantic.

Presently, TOPEX/POSEIDON is providing sea surface height observations with an unprecedented error budget of less than 5 cm (Fu et al. 1994), and the precision of those observations will even improve consid-

erably with increasing mission duration. Present-day ocean general circulation models, on the other hand, are run globally in realistic configuration on an eddy resolving grid and differences with TOPEX/POSEIDON data are shown to be on the order of 10 cm on large scales (Stammer et al. 1996). Methods have been developed that will allow the incorporation of altimeter observations into ocean general circulation models in an optimal yet practical way by accounting for errors in both data and models and by providing error estimates of the resulting fields (e.g. Stammer and Wunsch 1996). It can be anticipated that these methods will be used to obtain an estimate of the present ocean state by assimilating TOPEX/POSEIDON altimeter data jointly with information available from the diverse WOCE observations.

Acknowledgments. The material presented in this paper is part of my Ph.D. thesis. I am indebted to my advisor Jürgen Willebrand for many stimulating and challenging discussions. I am also grateful to W. Holland for providing his original QG model, and to R. H. Käse and G. Siedler for sharing their in situ hydrographic and current meter observations. Rohan Hughes helped with the English. I am obliged to three anonymous reviewers for their thorough comments, which substantially improved this manuscript. A grant from CRAY Research Inc. for model calculations on the CRAY X-MP of Kiel University is gratefully acknowledged. This study was supported by the BMFT (Grant 07 KFT 460). The final version of this manuscript was written at MIT under NASA Grant NAGW 1048.

REFERENCES

Anderson, D. L. T., and J. Willebrand, Eds., 1989: *Oceanic Circulation Models: Combining Data and Dynamics.* Kluwer Academic, 605 pp.

Berry, P., and J. Marshall, 1989: Ocean modeling studies in support of altimetry. *Dyn. Atmos. Oceans,* **13,** 269–300.

Capotondi, A., P. Malanotte-Rizzoli, and W. R. Holland, 1995a: Assimilation of altimeter data into a quasigeostrophic model of the Gulf Stream system. Part I: Dynamical considerations. *J. Phys. Oceanogr.,* **25,** 1130–1152.

——, W. R. Holland, and P. Malanotte-Rizzoli, 1995b: Assimilation of altimeter data into a quasigeostrophic model of the Gulf Stream system. Part II: Assimilation results. *J. Phys. Oceanogr.,* **25,** 1153–1173.

Charney, J. G., R. Fjörtoft, and J. von Neumann, 1950: Numerical integration of the barotropic vorticity equation. *Quart. J. Geophys.,* **2,** 237–254.

Chow, H. S., and W. R. Holland, 1986: Desciption of a quasigeostrophic multi-layer box ocean model. NCAR Internal Rep. [Available from NCAR, P.O. Box 3000, Boulder, CO 80307.]

DeMey, P., and A. R. Robinson, 1987: Assimilation of altimeter eddy fields in a limited-area quasigeostrophic model. *J. Phys. Oceanogr.,* **17,** 2280–2293.

Emery, W. J., W. G. Lee, and L. Magaard, 1984: Geographic and seasonal distribution of Brunt–Väisälä frequency and Rossby radii in the North Pacific and North Atlantic. *J. Phys. Oceanogr.,* **14,** 294–317.

Flierl, G. R., 1978: Models of vertical structure and the calibration of two-layer models. *Dyn. Atmos. Oceans,* **2,** 341–381.

Frankignoul, C., and P. Müller, 1979: Quasi-geostrophic response of an infinite beta-plane ocean to stochastic forcing by the atmosphere. *J. Phys. Oceanogr.,* **9,** 104–127.

Fu, L.-L., E. Christensen, M. Lefebvre, and Y. Menard, 1994: TOPEX/POSEIDON mission overview. *J. Geophys. Res.,* **99,** 24 369–24 382.

Fukumori, I., and C. Wunsch, 1991: Efficient representation of the North Atlantic hydrographic and chemical distribution. *Progress in Oceanography,* Vol. 27, Pergamon Press, 111–195.

——, J. Benveniste, C. Wunsch, and D. B. Haidvogel, 1993: Assimilation of sea surface topography into an ocean circulation model using a steady-state smoother. *J. Phys. Oceanogr.,* **23,** 1831–1855.

Ghil, M., and P. Malanotte-Rizzoli, 1991: Data assimilation in meteorology and oceanography. *Advances in Geophysics,* Vol. 33, Academic Press, 141–266.

Gordon, A. L., and W. F. Haxby, 1990: Agulhas eddies invade the South Atlantic: Evidence from Geosat altimeter and shipboard conductivity–temperature–depth survey. *J. Geophys. Res.,* **95,** 3117–3125.

Haines, K., 1991: A direct method for assimilating sea surface height data into ocean models with adjustments of the deep circulation. *J. Phys. Oceanogr.,* **21,** 843–868.

——, P. Malanotte-Rizzoli, R. E. Young, and W. Holland, 1993: A comparison of two methods for the assimilation of altimeter data into a shallow water model. *Dyn. Atmos. Oceans,* **17,** 89–133.

Hinrichsen, H.-H., M. Rhein, R. H. Käse, and W. Zenk, 1993: The Mediterranean water tongue and its chlorofluoromethane signal in the Iberian Basin in early summer 1989. *J.Geophys.Res.,* **98,** 8405–8412.

Holland, W., 1978: The role of mesoscale eddies in the general circulation of the ocean—Numerical experiments using a wind-driven quasi-geostrophic model. *J. Phys. Oceanogr.,* **8,** 363–392.

——, 1986: Quasigeostrophic modeling of eddy resolving ocean circulation. *Advanced Physical Oceanographic Numerical Modeling,* J.J. O'Brien, Ed., D. Reidel, 203–231.

——, and P. Malanotte-Rizzoli, 1989: Assimilation of altimeter data into an ocean circulation model: Space versus time resolution studies. *J. Phys. Oceanogr.,* **19,** 1507–1534.

——, V. Zlotnicki, and L.-L. Fu, 1992: Modeled time dependent flow in the Agulhas retroflection region as deduced from altimeter data assimilation. *S. Afr. J. Mar. Sci.,* **10,** 407–427.

Hurlburt, H. E., 1986: Dynamic transfer of simulated altimeter data into subsurface information by a numerical model. *J. Geophys. Res.,* **91,** 2372–2400.

Käse, R. H., J. F. Price, P. L. Richardson, and W. Zenk, 1986: A quasi-synoptic survey of the thermocline circulation and water mass distribution within the Canary Basin. *J. Geophys. Res.,* **91,** 9739–9748.

——, A. Beckmann, and H.-H. Hinrichsen, 1989: Observational evidence of salt lens formation in the Iberian Basin. *J. Geophys. Res.,* **94**(C4), 4905–4912.

Mellor, G. L., and T. Ezer, 1991: A Gulf Stream model and an altimetry assimilation scheme. *J. Geophys. Res.,* **96,** 8779–8795.

Moore, A., 1991: Data assimilation in a quasigeostrophic open-ocean model of the Gulf Stream region using the adjoint method. *J. Phys. Oceanogr.,* **21,** 398–427.

Müller, T. J., and G. Siedler, 1992: Multi-year current time series in the North Atlantic Ocean. *J. Mar. Res.,* **50,** 63–98.

Oschlies, A., and J. Willebrand, 1995: Assimilation of GEOSAT altimeter data into an eddy-resolving primitive equation model of the North Atlantic Ocean. *J. Geophys. Res.,* **101,** 14 175–14 190.

Robinson, M., R. Bauer, and E. Schroeder, 1979: Atlas of North Atlantic–Indian Ocean monthly mean temperatures and mean salinities of the surface layer. Ref. Publ. 18, Dept. of the U.S. Naval Oceanographic Office, Washington, DC.

——, M. A. Spall, L. J. Walstad, and W. G. Leslie, 1989: Data assimilation and dynamical interpolation in Gulfcast experiments. *Dyn. Atmos.Oceans,* **13,** 269–300.

Schlax, M. G., and D. B. Chelton, 1994: Detecting aliased tidal errors

in altimeter height measurements. *J. Geophys. Res.*, **99,** 12 603–12 612.

Schröter, J., U. Seiler, and M. Wenzel, 1993: Variational assimilation of Geosat data into an eddy resolving model of the Gulf Stream extension area. *J. Phys. Oceanogr.*, **23,** 925–953.

Stammer, D., 1992: "Uber die mesoskalige Variabilit" at im Atlantischen Ozean—Analyse und Assimilation von GEOSAT-Altimeterdaten. Dissertation an der Universit at zu Kiel, Berichte Inst. Meereskunde, Kiel, Germany. 210 pp.

——, and C. Wunsch, 1996: The determination of the large-scale ocean circulation from satellite altimetry using model boundary Green's functions. *J. Geophys. Res.*, **101,** 18 406–18 432.

——, H.-H. Hinrichsen, and R. H. Käse, 1991: Can meddies be detected by satellite altimetry? *J. Geophys. Res.*, **96,** 7005–7014.

——, R. Tokmakian, A. Semtner, and C. Wunsch, 1996: How well does a ¼° global circulation model simulate large-scale oceanic observations? *J. Geophys. Res.*, in press.

Verron, J., 1992: Nudging satellite data into quasigeostrophic ocean models. *J. Geophys. Res.*, **97,** 7479–7492.

——, and W. R. Holland, 1989: Impacts de données d'altimétrie satellitaire sur les simulations numériques des circulations générales océaniques aux latitudes moyennes. *Ann. Geophys.*, **7,** 31–46.

White, W. B., C.-K. Tai, and W. R. Holland, 1990: Continuous assimilation of simulated Geosat altimeter sea level into an eddy resolving numerical ocean model. Part 1: Sea level differences. *J. Geophys. Res.*, **95,** 3219–3234.

Willebrand, J., R. H. Käse, D. Stammer, H.-H. Hinrichsen, and W. Krauss, 1990: Verification of GEOSAT sea surface topography in the Gulf Stream extension with surface drifting buoys and hydrographic measurements. *J. Geophys. Res.*, **95,** 3007–3014.

Zenk, W., T. J. Müller, and G. Wefer, 1989: Barlavento-Expedition. Meteor-Ber. 89 (2), Inst. Meereskunde, Universität Hamburg. 238 pp.